

DYNAMICS OF THE TRANS-NEPTUNE REGION:
APSIDAL WAVES IN THE KUIPER BELT

William R. Ward

*Jet Propulsion Laboratory
California Institute of Technology
Pasadena, CA 91109*

and

*Lunar and Planetary Institute'
Houston, TX 77058*

Joseph M. Hahn

*Lunar and Planetary Institute
Houston, TX 77058*

September, 1997

Submitted to *Astron. J.*,

¹ Visiting Scientist

ABSTRACT

The role of **apsidal** density waves propagating in a primordial **trans-Neptune** disk (i. e., **Kuiper** belt) is investigated. It is shown that Neptune launches **apsidal** waves at its secular resonance near 40 AU which propagate radially outwards, deeper into the particle disk. The wavelength of **apsidal** waves is considerably longer than waves that might be launched at **Lindblad** resonances because the pattern speed, g_s , resulting from the apse precession of Neptune is much slower than its mean motion, Ω_s . If the early **Kuiper** Belt had a sufficient surface density, Σ , the disk's wave response to Neptune's secular perturbation would have spread the disturbing torque radially over a collective **scale** A , $\approx r(2\mu_d\Omega/|rdg/dr|)^{1/2}$, where $\mu_d \equiv \pi\sigma r^2/M_\odot$ and $\Omega(r)$, $g(r)$ are the mean motion and precession frequency of the disk particles. This results in considerably smaller eccentricities at resonance than had the disk particles been treated as non-interacting test particles. Consequently, **particles** are less apt to be excited into planet-crossing orbits, implying that the erosion **timescales** reported by earlier test-particle simulations of the **Kuiper** Belt may be underestimated. It is also shown that the torque the disk exerts upon the planet (due to its gravitational attraction for the disk's spiral wave pattern) damps the planet's eccentricity and **further** inhibits the planet's ability to erode the **disk**.

I. INTRODUCTION

In the past few years, the nature and dynamics of the Kuiper Belt has been a subject of considerable attention. Interest was sparked by the demonstration of Duncan, Quinn, and Tremaine that a trans-Neptune disk could provide a plausible source for short period comets (Duncan, *et al*, 1988). The discovery of the first Kuiper Belt object, 1992 QB₁, by Jewitt and Luu (1992) further accelerated efforts of both observers and modelers. Great advances in both machine capability and computing techniques led to a series of increasingly intensive numerical experiments on the dynamics of test particles in the Kuiper Belt region, e.g., Torbett, (1989), Gladman and Duncan, 1990; Holman and Wisdom (1993), Levison and Duncan (1993), Duncan, et al., (1995). These experiments made it clear that both secular and mean motion resonances play a major role in shaping the evolution of the Kuiper Belt. Analytical treatments of Kuiper Belt resonant dynamics have been provided by Morbidelli, *et al.* (1995) and Malhotra (1995, 1996).

To date, observations have yielded some 55 trans-Neptune bodies like 1992 QB₁. Based on the size of the sky area searched, estimates of the total population of such objects within 10 deg of the ecliptic and larger than 100 km is of order *few x 10⁴*. The total mass of the belt out to 50 AU from objects greater than 100 km in diameter is put at 0.06-0.25 M_⊕ (e.g., Jewitt *et al.*, 1996; Stern, 1996a).² However, these objects are far from uniform in their orbital characteristics. Most objects interior to 40 AU appear to reside in mean motion resonances with Neptune. These resonant orbits may be instrumental in preserving their occupants; it is well-known that Pluto enjoys such protection through its 3:2 resonance with Neptune, which prevents close encounters between these objects. Resonant objects typically have high eccentricities which may be evidence of resonance sweeping due to an outward migration of Neptune (Malhotra, 1997).

The formation and possible migration of Neptune requires a few Neptune masses of material to be scattered by that planet (Fernandez and Ip, 1984, 1986, 1996), suggesting a primordial Kuiper Belt considerably in excess of today's estimates if the belt extended smoothly into that region as well. Indeed, observations of extra-solar disks such as β Pictoris, reveal

²The recent discovery of 1996 TL₆₆ points to an additional scattered Kuiper belt component having a mass ~0.5 M_⊕, with orbits between 40 and 200 AU (Luu *et al.*, 1997)

remnant disks stretching far beyond the Sun-Neptune distance. Additionally, the existence of 100km sized objects such as QB_1 has been interpreted as evidence of a much more massive (i.e., $10-50M_{\oplus}$ between 30 and 50 AU) primordial Kuiper Belt. Stern and co-workers (Stern, 1995, 1996 a,b; Stern and Colwell, 1996) have pointed out that accretion in the *current* environment would not be possible due to (a,) high relative velocities that are erosive, and (b.) long collision time scales due to low number density. They argue that a much more massive and quiescent disk was needed in the past to account for the accretion of the largest objects so far observed, They postulate that this more massive disk may still exist beyond the gravitation influence of the giant planets, i.e., $r > 50$ AU, and that the low density region between there and Neptune may be highly depleted due to planetary perturbations, The current flux of short period comets, which are suggested to originate from chaotic layers bounding low order mean motion resonances (e.g., Malhotra, 1996), maybe the present day manifestation of this erosion process. Numerical experiments show that many test particles achieve Neptune crossing status within a Gyr (Levison and Duncan, 1993; Duncan, *et al.*, 1995) due to the action of secular and mean motion resonances, These results are reminiscent of studies of the stability of test particles between the major planets, (e. g., Franklin, *et al.*, 1989; Duncan, *et d.*, 1989; Weibel, *et u.*, 1990; Gladman and Duncan, 1990; Soper, *et al.*, 1991; Holman and Wisdom, 1993; and Grazier *et al.*, 1997.)

It is very tempting to extend the numerical and analytical studies of test particle behavior that have proved so valuable in explaining many of the emerging characteristics of the Kuiper Belt, to earlier epochs when the belt was presumed more massive. However, some caution is in order; test particle integrations are strictly valid only when there are no interactions with other particles in the disk. And yet a motivation for postulating a much more massive primordial disk is to speed up accretion rates, i.e., to insure more numerous collisions among the swarm. This may be a source of diffusion that is not included in the numerical models. Even more important are collective particle behaviors. These effects are long range and act continuously, not just during collisions. It is well known that a perturber orbiting in a fluid disk will launch density waves at resonances, and that the resulting fluid motions are quite unlike that of an isolated particle subject to the same perturbations. The question is When is a wave model a more reasonable approximation of a particle disk than the motions of non-interacting members? In this paper, we

explore that question for the particular case of a secular eccentricity resonance, and show that the necessary conditions for wave action are easily satisfied. The resultant disk behavior is that of a one armed spiral apsidal wave that propagates outwards, into the Kuiper Belt. Apsidal waves have previously been reported in Saturn's rings (Cuzzi *et al.* 1981) where the apsidal precession rate of the ring particles is commensurate with the mean motion of the satellite Iapetus. However, this is the first application we are aware of where the waves are launched from a true secular resonance, i.e., where the commensurability is between the apsidal rates of both perturber and disk particles. As we shall see, this has important implications for disk stirring, and for the orbit of the perturber launching the waves,

11. TEST PARTICLE MOTION

We begin by reviewing the behavior of a test particle orbiting near a secular resonance. A *Neptune-like* model will be employed in which a secondary of Neptune's mass is assumed to orbit a solar mass primary at a distance of $a_s = 30.1$ AU, with orbit period, $P_s = 165$ years, eccentricity, $e_s = 0.01$, and precession rate of the longitude of perihelion, $d\tilde{\omega}_s/dt \equiv g_s \approx g_8$, i.e., the frequency, 0.673 arcsec/yr, of the g_8 -mode of the solar system with corresponding period, $P_{\tilde{\omega}} = 1.93 \times 10^6$ years. This is the dominant term of the secular variation of Neptune's orbit (e.g., Applegate *et al.*, 1986; Knezevic *et al.*, 1991). To first order in e_s , and fourth order in e , the particle's eccentricity, the secular perturbation potential due to the secondary is (e.g., Brouwer and Clemence, 1964),

$$\phi_s = -\mu_s a^2 \Omega^2 \left\{ \frac{1}{2} b_{1/2}^{(0)} + \frac{e^2}{8} \alpha b_{3/2}^{(1)} + \frac{e^4}{128} \alpha^3 \frac{d^2}{d\alpha^2} b_{3/2}^{(1)} - \frac{1}{4} e e_s \alpha b_{3/2}^{(2)} \cos(\tilde{\omega} - \tilde{\omega}_s) \right\} \quad (1)$$

where a, Ω are the test particle's semimajor axis and mean motion, $\tilde{\omega}$ is its longitude of perihelion, $\mu_s \equiv M_s/M_\odot = 5.15 \times 10^{-5}$, $\alpha \equiv a_s/a < 1$ in the Kuiper disk, and

$$b_{j/2}^{(m)}(\alpha) \equiv \frac{2}{\pi} \int_0^\pi \frac{\cos(m\theta) \alpha^j d\theta}{(1 - 2\alpha \cos\theta + \alpha^2)^{j/2}} \quad (2)$$

are Laplace coefficients. The secondary and particle orbits are assumed to be coplanar, and the

elements subscripted s refer to the secondary. Since the pattern speed is the precession rate, g_s , the Jacobi integral averaged over short period terms is

$$J = E - \Omega_{ps} J_s = -(\alpha\Omega)^2/2 + \phi_s - g_s \alpha^2 \Omega \sqrt{1-e^2} \quad (3)$$

To the same accuracy as eqn (1), the normalized quantity $\hat{J} \equiv -2J/\mu_s (\alpha\Omega)^2$ can be written,

$$\hat{J} = Ae^4 + Be^2 - C \cos \varphi + D \quad (4)$$

where $\varphi \equiv \tilde{\omega} - \tilde{\omega}_s$ and,

$$A \equiv \frac{\alpha^3}{64} \frac{d^2 b_{3/2}^{(1)}}{d\alpha^2} - \frac{g_s}{4\mu_s \Omega}; \quad B \equiv \frac{\alpha}{4} b_{3/2}^{(1)} - \frac{g_s}{\mu_s \Omega}; \quad C \equiv e_s \frac{\alpha}{2} b_{3/2}^{(2)}; \quad D \equiv b_{1/2}^{(0)} + \frac{2g_s}{\mu_s \Omega} + \frac{1}{\mu_s} \quad (5)$$

A particle's semimajor axis does not vary due to secular forcing, so eqn (4) maybe used to construct phase space plots along curves of constant \hat{J} (level curves) to show how its eccentricity varies with the resonance angle φ . Figure 1 a shows the level curves for $\hat{J} - D$ when $\alpha = 1.37\alpha_s$, $a \equiv \alpha_s/\alpha = 0.731$, while Figure 1b displays $\hat{J} - D$ vs. e when $\sin(\tilde{\omega} - \tilde{\omega}_s) = 0$. The extrema, given by

$$\partial \hat{J} / \partial e = 4Ae^3 + 2Be \pm C = 0 \quad (6)$$

are the stationary points in Fig. 1a, Phase space trajectories tend to circle points ① and ②, while point ③ lies on the separatrix. Their positions are a function of the particle's semimajor axis. The two branches of eqn (6) can be computed numerically and are shown in Figure 2. If B is expanded about α_o where $g_s = (1/4)\mu_s \Omega \alpha b_{3/2}^{(1)}|_{\alpha_o}$, $B(\alpha_o) = 0$, it can be replaced by $-B'\Delta\alpha$, where $\Delta\alpha \equiv \alpha - \alpha_o$, and

$$B' \equiv \left. \frac{dB}{d\alpha} \right|_{\alpha_o} = \frac{1}{4\alpha^{3/2}} \left. \frac{d}{d\alpha} (\alpha^{5/2} b_{3/2}^{(1)}) \right|_{\alpha_o} \quad (7)$$

In this case, A and C can be evaluated at α_o as well with little error. The reference value α_o , is

now found from

$$\frac{1}{4}\alpha^5 h_{32}^{(1)}|_o = \frac{g_s}{\mu_s \Omega_s} = 1.67 \quad (8)$$

The LHS can be evaluated numerically from eqn (2) which reveals that eqn (8) is satisfied by the value $\alpha_o = 0.770$. This implies the resonance falls at $a_s/\alpha_o = 39.1$ AU, which agrees reasonably well with the location of the g_8 resonance found by Knezevic *et al.* (1991) when $I = 0$.

The equilibrium e's vs $\Delta\alpha$ are given by

$$\Delta\alpha = -2e^2 \left(\frac{A}{B'}\right) \mp \frac{1}{2e} \left(\frac{C}{B'}\right) \quad (9)$$

The negative branch turns around (i. e., $de/d\Delta\alpha = \infty$) at

$$e_* = \frac{1}{2} \left(\frac{C}{A}\right)^{1/3} \quad ; \quad \Delta\alpha_* = -\frac{3}{2} \left(\frac{A}{B'}\right) \left(\frac{C}{A}\right)^{2/3} \quad (10)$$

At a_o , the ratios are $A/B' = 0.324$, $C/A = 0.455 e_s$. Below e_* , the negative branch gives the eccentricity for ①; above e_* , it is e of ③, while the positive branch gives the eccentricity for ②. This application considers a planet that has recently formed from a cool disk composed of non-interacting bodies³, so the particles' forced eccentricities will likely lie along the lower portions of the Fig. 2 curves whenever they are multi-valued. The resulting maximum e on the positive branch is $e_{\max} = 2e = (C/A)^{1/3}$. The corresponding e-values are

$$e_* = 0.385 e_s^{1/3} \quad ; \quad e_{\max} = 0.769 e_s^{1/3} \quad (11)$$

For our adopted Neptune-like eccentricity ($e_s = 0.01$), these become (0.083, 0.166), respectively.

³For now, we assume that their free eccentricities due to gravitational relaxation of the disk can be neglected

III. COLLECTIVE RESPONSE

a. Collective Scale Length

Hahn, Ward, and Rettig (1996, hereafter HWR) have recently investigated a closely related problem: the effects of collective particle behavior on the trapping strength of m h order Lindblad resonances for particles experiencing orbital decay due to gas drag. They found that the density wave response of the particle disk of surface density, Σ , reduces the trapping strength by redistributing the angular momentum deposited at resonance over a collective scale length. This causes a strong reduction in the forced eccentricities. This length is roughly the distance, λ_* , that density waves can travel from resonance at their group velocity, $c_g = \pi G \Sigma / \kappa$, during the libration time of the resonance variable. The libration frequency is, $\dot{\phi} = |\kappa - m|\Omega - \Omega_{ps}|$, where Ω_{ps} is the pattern speed, and κ is the local epicycle frequency of the disk. In terms of the so-called frequency distance from resonance, $D \equiv \kappa^2 - m^2(\Omega - \Omega_{ps})^2 \approx 2\kappa(\kappa - m|\Omega - \Omega_{ps}|)$, the libration frequency is $\dot{\phi} \approx (\lambda/2\kappa)|dD/dr|$ with an average value equal to half the maximum. The libration time at distance λ_* becomes $\tau_{lib} \approx 1/\langle \dot{\phi} \rangle \approx 4\kappa/\lambda_* |dD/dr|$, where the derivative is evaluated where $D = 0$. Solving self-consistently, the scale length is of order,

$$\lambda_* \sim r \left| \frac{4\pi G \Sigma}{r^2 dD/dr} \right|^{1/2} \equiv r |2\epsilon|^{1/2} \quad (12)$$

The collective behavior smoothes out the perturbation, so that the torque cannot be *concentrated* on a very narrow annulus.⁴

HWR argued that there are two necessary conditions for wave action: (i.) there must be multiple particles present within the collective scale, and (ii.) their epicyclic radii must be less than the wavelength. We will tentatively assume these conditions are met, and check their validity *a posteriori*. Without collective behavior, the orbit crossing half-width⁵ of the resonance for a non-interacting, isolated particles (1P) can be estimated as $w = (\psi/r dD/dr)^{1/2}$, where ψ is the forcing

⁴Actually, eqn (12) underestimates the collective scale when λ_* becomes so long that dD/dr itself decreases significantly over that distance.

⁵This is the distance inside which orbits intersect 1 (is different than the amplitude half-width which varies as $\psi^{2/3}$).

function due to the perturber. The wave response will be linear with nested orbits if $\lambda_s > \omega$, i.e., when $\psi \lesssim 4\pi G\sigma r$. We show below that for a secular resonance, $\psi = O(e_s \mu_s r^2 \Omega^2)$. Introducing the so-called normalized disk mass, $\mu_d \equiv \pi \sigma r^2 / M_s = \pi G\sigma / r \Omega^2$, the linearity criterion reads, $4\mu_d \geq e_s \mu_s - 10^{-2} \mu_s$.

b. Wave Solution for Secular Resonances

From Goldreich and Tremaine [1980, eqn (5)], the secondary's potential is

$$\phi_s = \sum_{l=-\infty}^{\infty} \sum_{m=0}^{\infty} \phi_{l,m} \cos\{m\theta - m\Omega_s t - (l-m)\kappa_s t\} = \sum_{l=-\infty}^{\infty} \sum_{m=0}^{\infty} \phi_{l,m} \cos\{m\theta - (m-l)g_s t - l\Omega_s t\} \quad (13)$$

where the relationship

$$g_s \equiv d\tilde{\omega}_s/dt = \Omega_s - \kappa_s \quad (14)$$

has been used. To get the secular terms, which do not contain $\Omega_s t$, set $l = 0$. For $e_s \ll 1$, the largest term in any amplitude is proportional to $e_s^{|l-m|} = e_s^m$. For our purposes it is sufficient to retain only terms up to first order;

$$\phi_{\text{sec}} \approx \phi_{0,0} + \phi_{0,1} \cos(\theta - g_s t) \quad (15)$$

where, again from Goldreich and Tremaine (1980),

$$\phi_{0,0} = \frac{GM_s}{a_s} b_{1/2}^{(0)}(\beta) \quad ; \quad \phi_{0,1} = -e_s \frac{GM_s}{2a_s} \left[\frac{d}{dz} b_{1/2}^{(1)}(\beta) \right] \quad (16)$$

with $\beta \equiv r/a_s$, and the disk is assumed keplerian.⁶ (Henceforth, the $l = 0$ part of the subscript will be dropped.)

Following Shu (1984), all perturbed quantities are assumed of the form $X = X e^{i(\omega t - m\theta)}$, where $\omega \equiv m\Omega_{ps}$ is the forcing frequency, and the amplitude, ϕ' , of the disk potential perturbation in the vicinity of resonance can be found from

⁶It is more convenient to develop the wave formalism in terms of β . Note, however, that this is the reciprocal of a used in section II.

$$r \frac{d\phi'}{dr} + \frac{irD\phi'}{2\pi G\sigma} = -\left(r \frac{d\phi_m}{dr} - \frac{2\phi_m}{\Omega_{ps} - \Omega}\right) \equiv \psi \quad (17)$$

which is valid in the tight winding limit (Shu, 1984)⁷. For apsidal waves, $m = 1$, and the forcing frequency, $\omega = \Omega_{ps} \equiv g_s$. The $m = 0$ potential can be combined with the central potential, ϕ_{\odot} , and any *undisturbed* disk potential, ϕ_d , to determine the mean motion,

$$r\Omega^2 = \frac{d}{dr}(\phi_{\odot} + \phi_0 + \phi_d) \quad (18)$$

The solution to eqn (17) is

$$\phi' = \exp\left[-i \int \left(\frac{D}{2\pi G\sigma}\right) dr\right] \int_{r_e}^r \frac{\psi}{r} \exp\left[i \int \left(\frac{D}{2\pi G\sigma}\right) dr\right] dr \quad (19)$$

where for specificity we have set the inner boundary of the disk at the edge of the secondary's chaotic zone, i. e., $r_e - r_s = \mu^{2/7} r_s$ (Wisdom, 1980). For a secular resonance,

$$D = \kappa^2 - (g_s - \Omega)^2 \approx 2\Omega(g_s - g) \quad ; \quad \frac{dD}{dr}\Big|_{r_r} \approx -2\Omega \frac{dg}{dr}\Big|_{r_r} \quad ; \quad \epsilon = -\frac{\mu_d \Omega}{r dg/dr}\Big|_{r_r} \quad (20)$$

where $g(r) \equiv \Omega - \kappa$ is the apse precession rate of the disk particles with r_r locating the secular resonance where $D(r_r) = 0$, $g = g_s$.

If $\lambda_s \ll |r_r - r_e|, g_s / |dg/dr|_{r_r}$, so that the collective scale is small compared to both the distance to the disk edge and the scale over which a linear expansion, $D \approx (r - r_r) dD/dr|_{r_r}$, is reasonably good, eqn (19) can be written in terms of Fresnel integrals (e.g., Shu, 1984):

$$\phi' = q(2\pi|\epsilon|)^{1/2} \psi H_q(\xi) \quad (21)$$

⁷Note that Shu's sign convention is the reverse of Goldreich and Tremaine's. We can bring eqns. (13), (15) into compliance by multiplying the cosine arguments by -1.

where

$$q \equiv \text{sgn}\left(\frac{dl}{dr}\right) ; \quad \xi \equiv q \frac{(r-r_r)}{r_r \sqrt{2|\epsilon|}} ; \quad H_q = \frac{1}{\sqrt{\pi}} e^{-iq\xi^2} \int_{-\infty}^{\xi} e^{iq\eta^2} d\eta \quad (22)$$

If $g(r)$ decreases with heliocentric distance, $q = +$, and the direction of wave propagation is *outward, i.e.*, deeper into the Kuiper disk, This is opposite to the propagation of waves launched from Lindblad resonances in this region, Figure 3 shows a schematic diagram of an outward propagating, one arm, trailing spiral wave. The streamlines of the motion are ellipses whose lines of **apsides** rotate in a clockwise manner with increased distance from resonance,

To simplify ψ , note that $\phi_1 \propto \beta db_{1/2}^{(1)}/d\beta - b_{1/2}^{(1)}$ and make use of the fact that

$$\left(\beta \frac{d}{d\beta} + 2\right) \left(\beta \frac{db_{1/2}^{(1)}}{d\beta} - b_{1/2}^{(1)}\right) = \beta b_{3/2}^{(2)} \quad (23)$$

(Brouwer and Clemence, 1964) to find

$$\psi = \frac{e_s}{2} \beta b_{3/2}^{(2)} \mu_s \alpha_s^2 \Omega_s^2 \quad (24)$$

where the combination GM_s/a_s has been replaced by $\mu_s \alpha_s^2 \Omega_s^2$. Substituting into ϕ' yields

$$\phi' = \frac{e_s}{2} \mu_s \beta b_{3/2}^{(2)} \left(\frac{2\pi \mu_d \Omega}{|rdg/dr|}\right)^{1/2} \alpha_s^2 \Omega_s^2 H_q(\xi) \quad (25)$$

where only ξ is allowed to vary, all other quantities being evaluated at resonance. Downstream, $|H_q| \rightarrow 1$, and figure 4 shows $|\phi'|$ as a function of the disk's mass, where eqn (35) given below has been used for the derivative of g . Most of the driving occurs during the first wavelength, which increases with the square root of the disk mass, resulting in a similar increase in the amplitude, Also shown is the downstream value obtained from eqn (19) by numerical integration, allowing for variations in ψ , dl/dr , and σ that become more important at longer wavelengths. The driving is **mostly** limited to the distance over which the radial wavenumber

$$k(r) \equiv \frac{D}{2\pi G\sigma} \approx \frac{g_s - g}{\mu_d r \Omega} \quad (26)$$

increases rapidly with r . The concomitant shortening of the wavelength is necessary for a net angular momentum flux to develop, Figure 5 displays wavenumber, k , versus r for three values of the disk mass, $\mu_d(r_s) \equiv \mu_{d,s}$.⁸ In each case, the most rapid increase in wavenumber occurs within the first $\delta r \approx 0(10)$ AU. When the disk mass is so large that the first wavelength significantly exceeds this distance, the amplitude becomes limited by the steep part of the k -curves instead of the complete wavelength, and further mass increases are not effective. The oscillations in the amplitude curve (Fig. 4) from eqn (19) occur because the phase of the wave, at the nearly constant distance δr , changes with disk mass. The wavelength, $\lambda(r)$ - as defined by $\Phi(r+\lambda) - \Phi(r) = 2\pi$, where the phase, $\Phi(r) \equiv \int k dr$ - is shown in figure 7 for the same disk masses of figure 6, The curves start at 39,1 AU with the value of the first wavelength, This exceeds - 10 AU for disks with $\mu_d/\mu_s \geq 0(10)^1$.. However, even eqn (19) is an approximation because the derivation of eqn (17) ignores other slowly varying terms that may be significant at long wavelengths. Nevertheless, we see that eqn (25) is a useful approximation even up to $\mu_d \sim \mu_s$.

c. Wave Criteria

As advertised, we now return to the issue of whether the necessary conditions for wave action are met. First, we check to see when the epicycle radius, v_{disp}/Ω , due to the any dispersion velocity, v_{disp} , among the particles becomes comparable to the wavelength,

Disk stability requires a minimum dispersion velocity of $v_c = 1.07\pi G\sigma/\kappa \approx \mu_d(r\Omega)$ regardless of particle size (Toomre, 1969). Particles large enough that their escape velocities exceed this, will have dispersion velocities $v_{disp} = v_{esc}$. Call $v_{disp}/v_c \equiv Q$, so that $v_{disp} \approx \mu_d Q(r\Omega)$; the reader will recognize Q as the well known Toomre stability parameter, Setting $v_{disp}/\Omega = |k|^{-1}$, and assuming downstream behavior fork where g can be ignored, the location, β_Q , of the wave propagation barrier is given by

⁸As defined. $\mu_d \propto \pi \sigma r^2 / M$. vanes as r^{2-n} for a disk with surface density $\sigma \propto r^{-n}$

$$\beta_Q^n \sim (\Omega_s/g_s)Q_s \quad (27)$$

where $Q_s \equiv Q(r_s)$ is to be evaluated for an unperturbed disk at the distance of the secondary's orbit.

Kuiper disk objects with escape velocities comparable to stability minimum have radii, $R_c = \mu_d(r\Omega)(8\pi G\rho/3)^{-1/2} = 0.2(\mu_d/\mu_s)km$ for $\rho = 2 \text{ g/cm}^3$. Therefore, $Q_s \sim R/R_c = 5(\mu_s/\mu_d)(10^3/km)$ for $R > R_c$, and $\beta_Q^n = 2.3 \times 10^3(\mu_d/\mu_s)(R/km)^{-n}$, i.e., **-450** AU in a $n = 2$ Neptune mass disk composed of 10 km Kuiper objects, 140 AU if most of the mass is in 100 km objects. For $n = 3/2$, these distances increase to =1100 AU and =240 AU, respectively. [A better estimate of the distance to the Q-barrier can be found by including the Toomre reduction factor in the dispersion relation (Toomre, 1969; HWR; Hahn and Ward, 1997).]

Next check the requirement that there be multiple particles within a wavelength. Down stream, where k changes little during a given cycle, we can write

$$\lambda = \frac{2\pi}{k} \rightarrow 2\pi r \left(\frac{\mu_d \Omega}{g_s} \right) \approx 3.8 r_s \beta^{3/2-n} \left(\frac{\mu_{d,s}}{\mu_s} \right) \quad (28)$$

Because waves from a secular resonance can be extremely long, $\lambda = 0(10^2 \mu_d/\mu_s)$ AU, this requirement is easily satisfied, i.e., the typical spacing between particles is $\sim N^{1/2}$, where $N \equiv \sigma/M$ is the surface number density of objects of mass, M . QB₁ objects have masses of order $10^{-6}M_\oplus$; for this mass, $\lambda\sqrt{N} = 0(10^4)(\mu_d/\mu_s)^{3/2}$. If the bulk of the material is in smaller objects $R < 100km$, there is an additional factor $(10^2 km/R)^{3/2}$.

d. Resonance Site

The precession of a test particle's longitude of perihelion is given by

$$g \equiv \frac{d\tilde{\omega}}{dt} \approx \frac{-1}{ea^{2n}\Omega} \frac{\partial \Phi_T}{\partial e} \quad (29)$$

where $\Phi_T \equiv \Phi_s + \Phi_d + \Phi'$ is the sum of all the contributing potentials Using the disturbing

function eqn (1) to order e^2 , yields the familiar expression,

$$\left. \frac{d\tilde{\omega}}{dt} \right|_s \approx \mu_s \Omega \left[\frac{1}{4} \alpha b_{3/2}^{(1)} - \frac{1}{4} \left(\frac{e_s}{e} \right) \alpha b_{3/2}^{(2)} \cos(\tilde{\omega} - \tilde{\omega}_s) \right] \quad (30)$$

for the precession rate of an isolated test particle. The nominal resonance position, α_o , is where the first term equals the precession rate of the secondary, g., while the second term is used to ‘tune’ the rate to the resonance value for particles inside and outside of resonance. As the resonance is approached, the eccentricity (in this linear treatment) must diverge to shut off the second term when it is not needed, In section II, this singularity was removed by including ⁴ terms in the disturbing function. However, disk gravity will also remove the divergence as discussed below.

Ward (1981; see. also Heppenheimer, 1980) showed that an axisymmetric disk of surface density $\sigma \propto r^{-n}$ produces an additional potential,

$$\phi_d = -2\pi G \sigma r \sum_{j=0}^{\infty} \frac{(4j+1)[(2j)!]}{(2j+2-n)(2j-1+n)} \frac{1}{r^{2j}} \equiv -2\pi G \sigma r c_n \quad (31)$$

which also affects the precession rate, An easy way to show this is by writing $\kappa^2 = r d\Omega^2/dr + 4\Omega^2$ so that

$$\kappa^2 = r \frac{d\Omega^2}{dr} + 3\Omega^2 = \frac{1}{r^2} \frac{d}{dr} (r^3 \Omega^2) \quad (32)$$

Approximating $\kappa^2 - \Omega^2 = (\kappa + \Omega)(\kappa - \Omega) \approx -2\Omega d\tilde{\omega}/dt$, and using eqn (18) allows one to find the precession rate. The central $1/r$ potential can be ignored because it cannot produce precession, while the contribution from ϕ_s is already included in eqn (30), The addition contribution from the undisturbed disk is,

$$\left. \frac{d\tilde{\omega}}{dt} \right|_d = \frac{-1}{2r^2 \Omega} \frac{d}{dr} \left[r^2 \frac{d\phi_d}{dr} \right] = -C_n \mu_d \Omega \quad (33)$$

that must be added to the RHS of eqn (30), where $C_n \equiv (n-1)(2-n)c_n$ For a wide range of n ,

($\alpha_n = O(1)$), and eqn (33) describes **apsidal line regression**, which shifts the resonance location inward toward the secondary (Ward, 1981, see also Levison *et al.*, 1996).

Remembering that wave behavior of the disk results in a much reduced eccentricity compared to the isolated particle case, the second term in eqn (30) can no longer vanish due to a divergence of e . On the other hand, there is an additional part of the potential due to the spiral wave, $(\mathcal{S})'$, yet to consider. It is shown in the appendix that these two **non-axisymmetric** terms cancel, leaving

$$\frac{1}{4}\alpha^{5/2}b_{3/2}^{(1)} - C_n\left(\frac{\mu_{d,s}}{\mu_s}\right)\alpha^{n-1/2} = \frac{g_s}{\mu_s\Omega_s} \quad (34)$$

as the resonance condition,

The disk correction to the resonance location is small for disks of moderate mass, i.e., $\mu_{d,s} \lesssim \mu_s$. In this case, the resonance condition is approximately that used in section II, and $r_r \approx r_o$. The gradient of the precession frequency is then,

$$r\frac{dg}{dr} \approx -\frac{1}{4}\mu_s\Omega_s\alpha\frac{d}{d\alpha}[\alpha^{5/2}b_{3/2}^{(1)}(\alpha)] \equiv -\Gamma(\alpha)g_s \quad (35)$$

where $\Gamma(\alpha)$ is a function of semi-major axis, but does not depend explicitly on Laplace coefficients (Appendix B). For $a = 0.770$, $\Gamma = 9.13$.

e. Eccentricities

In the tight winding limit, the fluid disk's radial velocity is $U \approx \phi'\Omega/2\pi G\sigma$ (e.g., HWR), while the eccentricity is

$$e_{dw} \approx \left|\frac{U}{r\Omega}\right| \approx \frac{1}{4}e_s\mu_s\alpha b_{3/2}^{(2)}(\alpha)\left(\frac{2\pi}{\mu_d}\right)^{1/2}\left(\frac{\Omega}{|rdg/dr|}\right)^{1/2}|H_s| \quad (36)$$

with the RHS being evaluated at resonance. In (36) the Laplace coefficient is written in terms of $a \equiv 1/\beta$, by making use of the identity $b_{j/2}^{(m)}(\beta) = \alpha' b_{j/2}^{(m)}(\alpha)$. Substituting eqns (8) and (35) and evaluating $b_{3/2}^{(2)}(\alpha_o) = 11.19$ yields

$$e_{dw} \approx 1.1 e_s \left(\frac{\mu_s}{\mu_d} \right)^{1/2} |H_s| \quad (37)$$

Eqn (36) is compared to test particle behavior in figure 2 for the case $\mu_d = \mu_s$. The collective response of the disk suppresses the particles' eccentricity below the isolated particle value, $e_{\max} = 0.769 e_s^{1/3}$, when $\mu_d/\mu_s \geq 2.4 e_s^{4/3}$, which for $e_s = 0.01$, reads 5×10^{-3} . Hence, for **low** mass disks with $\mu_d \leq 10-2 \mu_s$, collective behavior is not important. However, for higher mass the forced eccentricity is reduced by the wave action, For a disk mass comparable to Neptune, the full amplitude eccentricity is $e_{dw} = 0.011$, which is down by a factor, $e_{dw}/e_{\max} = 1.4 e_s^{2/3} = 0.065 \approx 1/15$. At the resonance itself, $|H_s| = 1/2$, and the eccentricity is only half its downstream value,

f. Secondary's Orbit.

The reaction torque, $T_s = -T = r\dot{\phi}^2/4G$, on the secondary can have important effects on its orbit (e.g., Goldreich and Tremaine, 1980). The secondary's angular momentum and energy are: $L = M_s a_s^2 \Omega_s (1 - e_s^2)^{1/2}$, $E = -M_s (a_s \Omega_s)^2 / 2$. Differentiating with respect to time, and rearranging yields, $\dot{a}_s/a_s = -\dot{E}/E$, $\dot{e}_s/e_s = -e_s^{-1} (1 - e_s^2)^{1/2} [\dot{L}/L + \dot{E}/2E]$, where $\dot{L} = T_s$. Since a wave potential appears **stationary** in a reference frame rotating at its pattern speed, the rates of change are related as $\dot{E} = \Omega_{ps} \dot{L}$, by virtue of the Jacobi constant. From this, semi-major axis and eccentricity variation rates can be derived,

$$\frac{\dot{a}_s}{a_s} = \frac{2T_s}{M_s a_s^2 \Omega_s} \left(\frac{\Omega_{ps}}{\Omega_s} \right) \quad ; \quad \frac{\dot{e}_s}{e_s} = \frac{-T_s}{M_s e_s^2 a_s^2 \Omega_s} \left[1 - \left(\frac{\Omega_{ps}}{\Omega_s} \right) \sqrt{1 - e_s^2} \right] \quad (38)$$

Substituting the torque and pattern speed, g_s , for the secular resonance in the c equation yields

$$\frac{1}{e_s} \frac{de_s}{dt} \Big|_{\text{sec}} = -\frac{\pi}{4} \beta^{3/2} (b_{3/2}^{(2)}(\beta))^2 \mu_d \mu_s \Omega_s \left(-\frac{\Omega_s}{rdg/dr} \right) \sim -1.66 \mu_d \mu_s \Omega_s \left(\frac{\Omega_s}{g_s} \right) \quad (39)$$

From (38), it follows that the ratio $|\dot{e}_s/e_s|/|\dot{a}_s/a_s| = [\Omega_s/\Omega_{ps} - (1-tJ32)12]/2t \sim \approx \Omega_s/2e_s^2 g_s \gg 1$,

so that the **semimajor** axis changes little during the decay of the eccentricity Eqn (39) is to be compared with the excitation rate from Lindblad resonances (Goldreich and Tremaine, 1980, Ward, 1988),

$$\frac{1}{e_s} \frac{de_s}{dt} \sim \frac{m_{\max}^4}{12\pi} \mu_d \mu_s \Omega_s \left[\frac{19}{4} K_1(4/3) + 5K_o(4/3) \right]^2 - 0.048 \mu_d \mu_s \Omega_s \left(\frac{a_s}{\Delta r} \right)^4 \quad (40)$$

where m_{\max} is the largest order Lindblad resonance falling in a disk with an inner edge a distance $Ar \equiv r_e - a_s$ from the secondary. Unlike $(\dot{e}_s/e_s)_{\text{sec}}$, eqn (40) falls off rapidly as Ar is increased. Thus, Lindblad resonances cannot prevent the decay of the eccentricity if the distance to the inner edge exceeds $Ar - 0.4a_s (g_s/\Omega_s)^{1/4} \approx 0.04a_s - 1.2 \text{ AU}$, which is comparable to the edge of the chaotic zone. When the secular resonance dominates, e decays with a characteristic time scale of $\tau_{\text{decoy}} \sim 5.2 \times 10^5 (\mu_s/\mu_d)$ years, and the disk torque on the secondary quickly damps its orbital eccentricity!

V. DISCUSSION

Figure 7 plots the perturbed surface density for $\mu_d/\mu_s = 1$, found from the WKB solution to Poisson's equation for ϕ' (e.g., Goldreich and Tremaine, 1978, 1979),

$$\sigma' = \frac{l}{2\pi G r^{1/2}} \frac{d}{dr} (r^{1/2} \phi') \quad (41)$$

The long wavelength keeps the response linear at launch because non-linear forcing only occurs when $e_{\text{dw}} \geq \lambda_*$ (e.g., HWR), for which $\mu_d/\mu_s \leq \sqrt{\pi} e_s \alpha h_{3/2}^{(2)}/4 - 0.04$. For larger disks, the forcing at resonance is linear.

Non-linearity *can* develop downstream if the waves wind up and/or the surface density drops sufficiently. The fractional perturbation of the wave, σ'/u , is found from the conservation

⁹Actually, the torque from an interior secular resonance would excite the eccentricity (Hahn and Ward, 1997). but here we assume that the interior planetesimal disk has been swept up by planet formation by the time Neptune forms

of angular momentum luminosity (Toomre, 1964, Goldreich and Tremaine, 1978)

$$|\mathcal{G}| = m\pi^2(ir)\left|\frac{\sigma'}{k}\right|^2 = \frac{m\sigma\phi'^2}{4G} \approx \frac{m\pi^2\sigma\psi^2}{|rdI/dr|} \Big|_o \quad (42)$$

where the RHS is to be evaluated at resonance. For our Neptune-like model, the fractional density perturbation is

$$\frac{u'}{o} = e_s \alpha_o^{(2n+5)/4} b_{3/2}^{(2)}(\alpha_o) \left(\frac{\mu_s}{\mu_{d,s}}\right)^{3/2} \left(\frac{g_s}{\mu_s \Omega_s}\right)^{1/2} \left(\frac{\pi}{8\Gamma}\right)^{1/2} \left(\frac{r}{a_s}\right)^{2(n-1)} \approx 1.1 e_s \left(\frac{\mu_s}{\mu_{d,s}}\right)^{3/2} \alpha_o^{n/2} \left(\frac{r}{a_s}\right)^{2(n-1)} \quad (43)$$

For $n = 2$, σ'/σ approaches unity at $r \approx 1.1 e_s^{-1/2} (\mu_{d,s}/\mu_s)^{3/4} a_s$, which for $e_s = 0.01$, $a_s = 30.1$ AU, $\mu_{d,s} = \mu_s$; reads $r = 330$ AU. Non-linear waves may shock dissipate, depositing their energy and angular momentum in remote regions of the disk, The large wavelengths of apsidal waves may also render them detectable in extra-solar disks. This issue is to be addressed in a follow-on paper (Hahn and Ward, 1997).

Long term test particle integrations have shown that Neptune will eject bodies with $q < 35$ AU over timescales < 109 years (Duncan *et al.*, 1995), The removal of test particles with $a < 35$ AU is likely assisted by Neptune's mean motion resonances. However it appears that the mean motion resonances must play a lesser role in stirring and depleting the more distant parts of a Kuiper Belt composed of test particles. The Jacobi constant for a particle at an $m+1:m$ mean motion resonance has the same form as eqn. (3) but with $A \approx 3(m+1)^{2/4}$ and $C \approx 8m\mu_s/5$, so the particle's maximum eccentricity is $e_{\max} = (C/A)^{1/3} \approx (2.1 \mu_s/m)^{1/3} (1+1/m)^{-2/3} \approx 0.05m^{-1/3} (1+1/m)^{-2/3}$, and its perihelion is $q = a_s [(1+1/m)^{2/3} - 0.05/m^{-1/3}] > 35$ AU for all of the $m \leq 3$ resonances that lie beyond 35 AU. Therefore, it appears that the g_8 resonance is the most significant in-plane perturbation exerted by Neptune in the more distant part of the Kuiper Belt. In section II, it was confirmed that the perturbations exerted on a massless test particle at the g_8 resonance are sufficiently vigorous to excite its eccentricity and lower its perihelion below 35 AU for a range of semi-major axes. Consequently, this resonance may act as a particle sink in the current Kuiper Belt since nearby particles may diffuse into the resonance

Although long-term test particle integrations shed light on the recent behavior of the

Kuiper Belt, they appear less credible for its earliest stage, when its mass may have been much larger. The self-gravity of the disk cannot be ignored, and the particles can respond in a collective (i.e., wave) mode. At a secular resonance, the necessary conditions for wave action are easily satisfied, and Neptune launches apsidal waves that propagate outward into the Kuiper Belt. *The wave response spreads Neptune's torque over the collective scale, resulting in significantly lower particle eccentricities than predicted by the isolated particle treatment.* The particle motions are coherent and nested, and do not contribute to a dispersion velocity. Since test particle simulations do not consider particle-particle interactions, they fail to account for this transport property of density waves and, thus, the reliability of their findings is uncertain. For a secular resonance at 39 AU in a $\mu_d \approx \mu_{Neptune}$ disk, particles acquire insufficient eccentricities to have their perihelia within 35 AU of Neptune. Indeed, it seems problematic whether this secular resonance could contribute significantly to the depletion of the Kuiper Belt in an early, high mass stage, unless it somehow acts in concert with other resonances in an as yet unknown manner. This caveat may also apply to other situations treated by test particle integrations, such as the depletion of the asteroid belt and of planetesimals between the planets.

The lowest mass estimate of the primordial Kuiper Belt obtained via a test particle simulation is given in Fig. 8 of Duncan *et al.* (1995), who require an initial number density profile of $n(r) \sim 3 \times 10^6 \times (40 \text{ AU}/r)^2 \text{ particles/AU}^2$ to account for the present flux of Jupiter family comets into the inner Solar System. This implies an initial surface density of $\sigma \sim 0.06 (R/10 \text{ km})^3 \text{ gm/cm}^2$ or $\mu_d/\mu_s \sim 0.7 (R/10 \text{ km})^3$ at 40 AU, assuming a mass density of 1 gm/cm^3 . Since the bulk of these objects must be comet-sized, R is likely 1-10 km. Inserting this disk mass into the discussion of section IIc shows that even at the low end, the criteria for apsidal wave propagation are still met, although the waves may be non-linear. Again, these models do not allow for the de-focusing of the planet's disturbance at resonance due to the disk's self-gravity, and as a result the erosion timescales reported in Duncan *et al.* (1995) may be underestimated.

A substantial disk is required by models in which the giant planets migrate (e.g., Fernandez and Ip 1983, Malhotra 1995, 1996). For instance, Malhotra (1997) estimates that $\sim 35 M_{\oplus}$ of disk material distributed between the giant planets is necessary to expand

Neptune's orbit such that Pluto is captured at a mean motion resonance with its eccentricity pumped up to the observed value. If one spreads this amount of disk material between the giant planets as per an r^{-2} surface density distribution, and then extrapolates additional mass beyond Neptune's orbit¹⁰, then the inferred disk mass is $\mu_d/\mu_s \approx 0.6$,

A similarly massive primordial Kuiper Belt has been postulated by Stern (1996), who prefers $\approx 10-50M_{\oplus}$ of material between 30 and 50 AU (i.e., $\mu_d/\mu_s \approx 0.6$ to 3 for a r^{-2} surface density distribution) in order to collisionally assemble ≈ 100 km sized QB_1 -type Kuiper Belt objects prior Neptune's formation. In this scenario, Neptune forms after $\approx 10^8-9$ years and is then presumed to stir up the disk so much that further growth of QB_1 objects is halted. Although Neptune's shorter wavelength Lindblad waves will be shut off once the particles achieve that size, Neptune's apsidal waves still propagate. If this scenario is to succeed then it remains to be demonstrated whether Neptune can actually stir up this massive disk in order to shut off its apsidal waves, truncate particle growth at QB_1 sizes, and also deplete the disk to its current low-mass state,

Neptune's ability to erode a massive primordial disk is further inhibited by the torque that the disk exerts upon the planet. The torque between planet and disk is surprisingly strong because the long wavelengths allow the disk to couple to the forcing potential over large distances. As a result, Neptune's eccentricity damping timescale could be quite short as compared to the age of the Solar System, which obviously contradicts Neptune's finite (though curiously low) eccentricity. One possible resolution to this dilemma is that an extended Kuiper Belt beyond 50 AU does *not* exist, and the dropoff in surface density past Neptune is a remnant of the true edge of the primordial planetesimal disk. Alternatively, sufficient erosion of the disk beyond the secular resonance could shut down the wave response. However, we have seen that collective behavior may inhibit erosion, so a better treatment of this problem, including Lindblad resonances, is needed. Still another possibility is that waves reflect off the Q-barrier or a real disk edge before damping, and return their energy and angular momentum to the resonance zone. At any rate, the requirement that Neptune's present eccentricity - or more precisely the amplitude of the g_8 mode

^{10A} Although it should be said that extending the disk well beyond Neptune is an additional assumption not required by the migration hypothesis

- be finite could be used to place a rather stringent constraint on the mass and distribution of the current Kuiper Belt We shall address this important topic in a follow-on paper.

APPENDIX A

To calculate the effect of the wave potential on a particle's precession rate, Gauss's form of Lagrange's equation is employed

$$\frac{d\tilde{\omega}}{dt} = \frac{1}{p} [F_r \cos f + F_\theta (\frac{r}{p} + 1) \sin f] \quad (44)$$

where f is the true anomaly, F_r, F_θ are radial and azimuthal perturbation forces, and $p \equiv u(1 - e^2)$. In the tight winding limit, $|\partial\phi'/\partial r| \gg (1/r) |\partial\phi'/\partial\theta| \Rightarrow |F_r| \gg |F_\theta|$, so we drop the second term and set .

$$F_r \approx \text{Re} \{ e^{-i(f - \tilde{\omega} - \tilde{\omega}_s)} (-d\phi'/dr) \} \quad (45)$$

The wave potential satisfies eqn (17). For a test particle at resonance, $D = 0$, and the orbit averaged contribution of the wave potential to the precession rate becomes,

$$\left. \frac{d\tilde{\omega}}{dt} \right|_w = \frac{\Psi}{2ea^2\Omega} \cos(\tilde{\omega} - \tilde{\omega}_s) \quad (46)$$

Substituting for Ψ reveals that eqn (32) cancels the problematic (e_s/e) -term in eqn (30)

APPENDIX B

The derivative of g is

$$r \frac{dg}{dr} = -\frac{1}{4} \mu_s \Omega_s \alpha^5 \left[\frac{r^{-5}}{2} + \alpha \frac{d}{d\alpha} b_{3,2}^{(1)} \right] \quad (47)$$

From Brouwer and Clemence (1964),

$$\alpha \frac{d}{d\alpha} h_{3/2}^{(1)} \cdot \frac{1 + 4\alpha^2}{1 - \alpha^2} h_{3/2}^{(1)}, \quad -\frac{\alpha}{\alpha^2} h_{3/2}^{(2)} \quad (48)$$

The ratio of Laplace coefficients is given by the continued fraction (Brouwer and Clemence, 1964)

$$\frac{b_{3/2}^{(2)}}{b_{3/2}^{(1)}} = \cfrac{5a}{41 - \cfrac{a^2}{1 - \cfrac{b a^2}{1 - \cfrac{c a^2}{1 - \cfrac{d \alpha^2}{\dots}}}}} \equiv p_{3/2}^{(2)} \quad (49)$$

with $a = -1/8$, $b = 7/16$, $c = 1/16$, $d = 3/8$, etc. Combining and using eqn (8) leads to

$$r \frac{dg}{dr} = -g \left[\frac{7 - 2\alpha p_{3/2}^{(2)} + 3a^2}{2(1 - a^2)} \right] \equiv -g l'(a) \quad (50)$$

For $a = 0.770$, $p_{3/2}^{(2)} = 0.874$ and $\Gamma = 9.13$.

ACKNOWLEDGMENTS

The research described in this paper was carried out, in part, at the Jet Propulsion Laboratory, California Institute of Technology under contract with the National Aeronautics and Space Administration. W.R.W. also thanks the Lunar and Planetary Institute for their hospitality during a portion of this effort. This paper represents contribution xxx from the Lunar and Planetary Institute, which is operated by the Universities Space Research Association under NASA contract NAGW-4575.

REFERENCES

- Applegate, J. H., Douglas, M. R., Gursel, Y., Sussman, G. J., and Wisdom, J., 1986. *Astron. J.*, 92, 176,
 Brouwer, D., and Clemence, G. M., 1961 *Methods of Celestial Mechanics*, Academic Press, New York

- Cuzzi, J N , Lissauer, J J . and Shu, F t 1., 1981, *Nature*, **292**, 703.
- Duncan, M. J., T Quinn, and S Tremaine, 1988. *Astrophys.J. Lett.*, **328**, L69.
- Duncan, M.J., Levison, H.F , and Budd, S. M., 1995, *Astron.J.*, 110, 3073
- Fernandez, J. A., and Ip, W.-H., 1983. *Icarus*, 54, 377.
- Fernandez, J. A., and Ip.W.-H., 1984, *Icarus*, 58, 109,
- Fernandez, J. A., and Ip, W.-H , 1996, *Planet. & Space Sci.* 44,431.
- Franklin, F., and Lecar, M., 1997. *Icarus*, in press.
- Franklin, F., Lecar, M , and Soper, P., 1989 *Icarus*, 79, 223.
- Gladman, B., and Duncan, M, 1990, *Astron.J.*, **100**, 1680.
- Goldreich, P., and Tremaine, S., 1978. *Icarus*, 34,240.
- Goldreich, P., and Tremaine, S., 1980. *Astrophys.J.*, 241,425.
- Grazier, K. R., Newman, W.I., Kaula, W. M., and Hyman, J. M., 1997. Preprint.
- Hahn, J. M., and Ward, W. R., 1997. In preparation.
- Hahn, J. M., Ward, W. R., and Rettig, T. W., 1995. *Icarus*, 117,25.
- Heppenheimer, T. A., 1980. *Icarus*, 41, 76.
- Holmann, M. J., and J. Wisdom, 1993. *Astron. J.*, **105**, 1987.
- Jewitt, D. C., and J. X. Luu, 1992. *IAU Circ.* **5611**.
- Jewitt, D. C., J. X. Luu, and Chen, 1996. *Astron. J.* 112, 1225.
- Knezevic, Z., Milani, A., Farinella, P. Froeschle, C., and Froeschle, C., 1991. *Icarus*, 93, 316.
- Levison, H.F., and M. J. Duncan, 1993. *Astrophys.J. Lett.*, **406**, L3.
- Levison, H.F., Stern, S.A., and Duncan, M.J., 1997. *Icarus*, in press.
- Luu, J. X. *et al.* 1997. *Nature* 387, 573.
- Malhotra, R., 1995. *Astron. J.*, 110,420.
- Malhotra, R., 1996. *Astron. J.* 111, 504.
- Molhotra, R, 1997. *Planet. & Sp.Sci.*, in press..
- Morbidelli, A., Thomas, F., and Moons, M., 1995. *Icarus*, **118**, 322.
- Shu, F. H., 1984. In *Planetary Rings*, (Eds. Greenberg, R, and Brahic, A., Univ. Of Arizona Press, Tucson) pp. 513-561.
- Soper, P., Franklin, F , and Lecar, M., 1990 *Icarus*, 87,265.

Stern, S A , 1995. *Astron. J.*, **110**, 856.

Stem, S A , 1996a In *Completing the Inventory of the Solar System*, (Eds Rettig, T. W, and Hahn, J M , ASP Conf Series) pp 209-232

Stem, S. A, 1996b. *Astron. J.* , 112, **1203**.

Stern, S. A., and Colwell, J, E., 1997. *Nature*, in press.

Toomre, A., 1964. *Astrophys. J.*, **139**, 1217,

Torbett, M. V., 1989. *Astron. J.*, 98, 1477,

Ward, W. R, 1981, *Icarus*, 47,234,

Ward, W. R., 1988. *Icarus*, 73, 330.

Ward, W. R. And Hahn, J. M., 1997. In preparation,

Weibel W. M., Kaula, W. M., and Newman, W. I., 1990. *Icarus*, 83, 382,

Wisdom, J., 1980. *Astron. J.*, **85**, 1122.

FIGURE CAPTIONS

Fig. 1. (a) The \hat{J} level curves for eqn (4). Each curve is a polar plot of eccentricity e versus resonance angle φ for particles having the same semi-major axis $a = 0.731$, but different values of \hat{J} (i. e., different free eccentricities). This and subsequent figures assume Neptune's mass and orbit. (b) The solid curve shows $\hat{J}-D$ versus $e \cos \varphi$ (D is constant) when $\sin \varphi = 0$, and the dashed lines identify the values of $\hat{J}-D$ for each of the level curves in the upper figure; the lowest dashed line refers to the smallest bean-shaped orbit in (a) while the upper dashed line is for the outermost orbit.

Fig.2. The particle's forced eccentricity e versus semi-major axis (note that a increases to the left). The curve labeled ② is the numerical solution to eqn (4) with $\cos \varphi = +1$, while the $\cos \varphi = -1$ solution has an upper ③ segment and a lower ① segment. The lower portions of the ②-curve left of e_{\max} and the lower segment ① represent the eccentricities that are likely adopted by a disk of initially cold particles The dot indicates the maximum eccentricity $e_{\max} = 0.17$ occurs a distance $\Delta \alpha = -0.01$ from the resonance site α_0 , consistent with the estimates given by eqns (10) and (11). Also shown is the $e(\alpha)$ necessary for the perihelion

distance, $q = 35$ AU

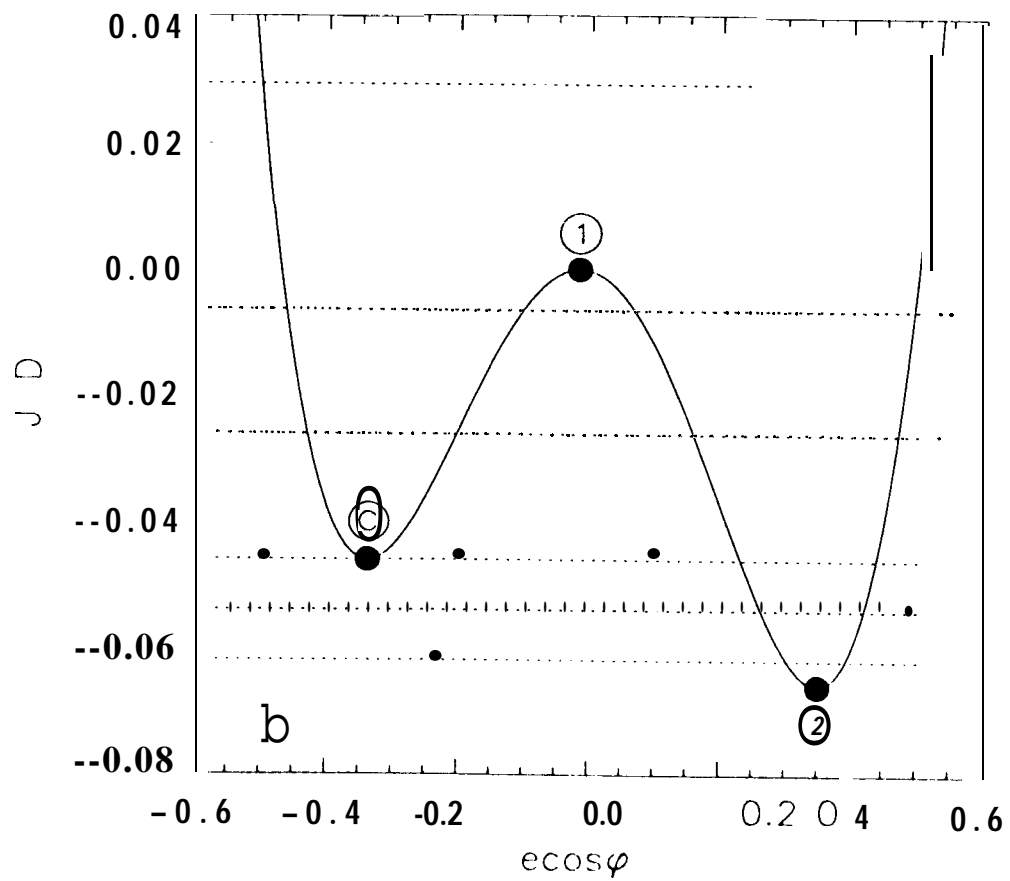
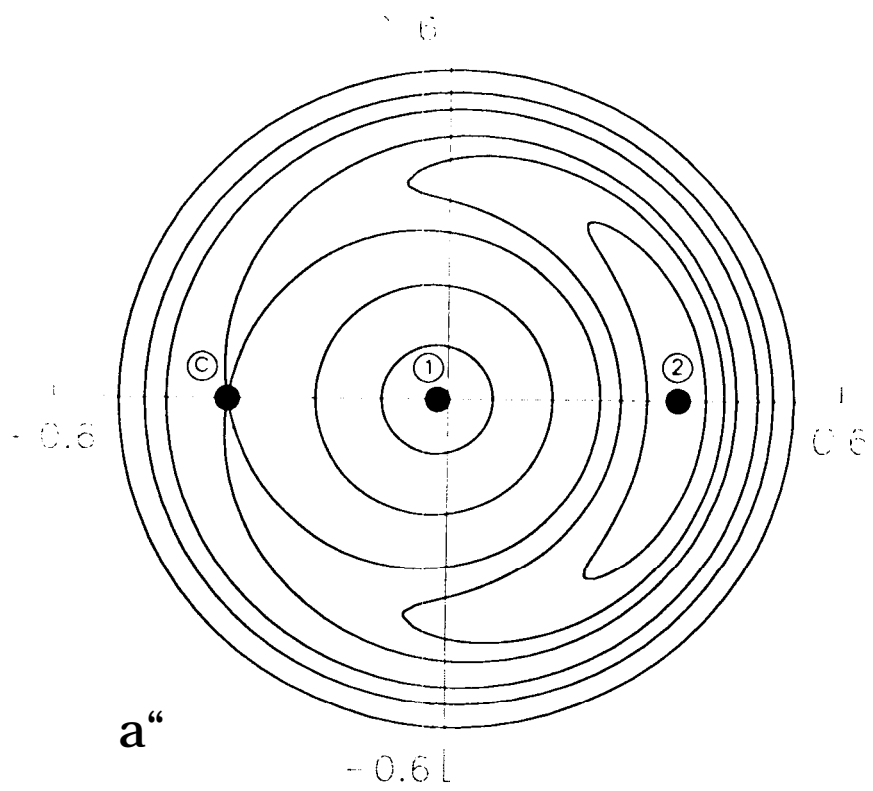
Fig 3. Schematic diagram of $m = 1$ elliptical streamlines oriented to produce a one-armed spiral, Cross denotes the position of the primary. (From Adams, *et al.*, *Astrophys. J.* 347, 959.)

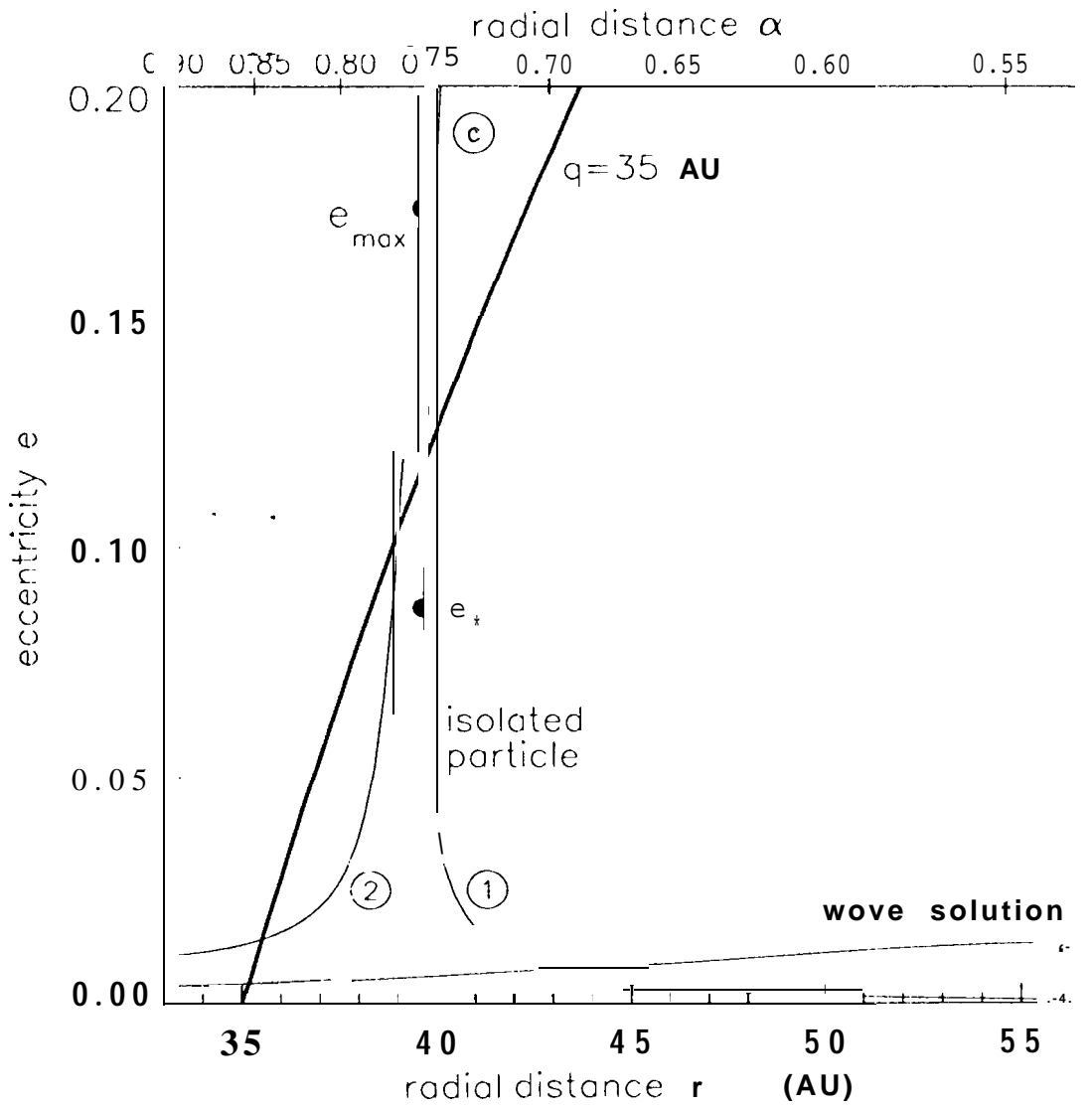
Fig. 4. Absolute value of the downstream amplitude, $|\phi'|$, of the disk wave potential in units of $e_s \mu_s (a_s \Omega_s)^2$. Dashed curve is the small wavelength (low disk mass) solution, eqn (25), Solid curve shows the numerical integration of eqn (19), taking into account a finite lower boundary, and variations in $\psi, dD/dr, \sigma$ with r , which become more important as the wavelength increases.

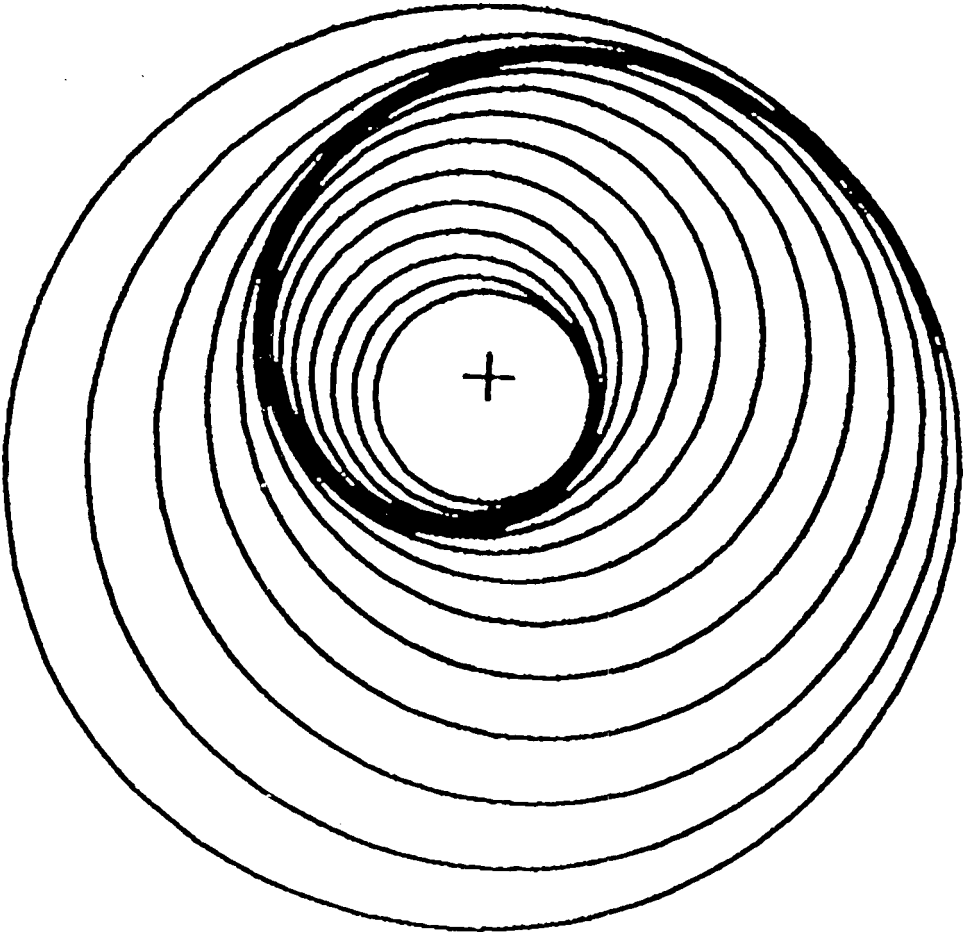
Fig. 5. Wavenumber as given by the dispersion relationship, $k = D/2\pi G \sigma \sim (g_s - g)/\mu_d (r\Omega)$, which increases rapidly as $g(r)$ drops, and then more slowly as $r^{n-3/2}$, for a $\sigma \propto r^{-n}$ disk, Case shown is for $n = 2$. Curves are parameterized by the disk to secondary mass ratio with μ_d evaluated at a_s .

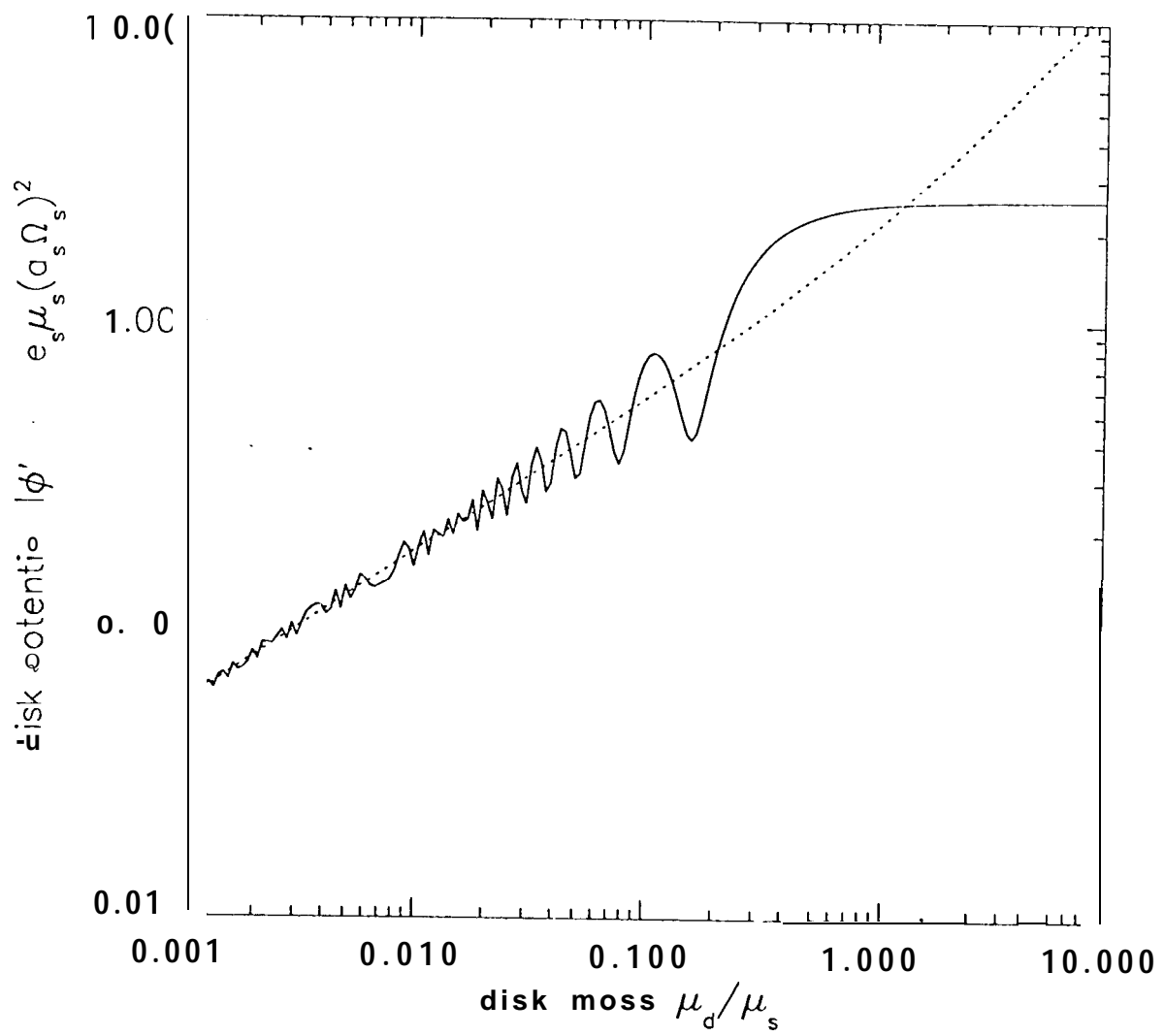
Fig. 6. Wavelength, $\lambda(r)$, defined by the relationship, $\int_{\cdot}^{r+\lambda(r)} k dr = 2\pi$, for the same cases shown in figure 5. The beginning of each curve marks the value of the first wavelength, For higher mass disks, the first wavelength extends beyond the rapid rise in σ so that a precipitous drop in wavelength is not observed,

Fig. 7. Surface density perturbation in an $n = 2$ disk for an one-armed trailing apsidal wave generated in an extended Kuiper Belt by a secondary at 30.1 AU with normalized disk and secondary masses comparable to Neptune's mass. White circle indicates the resonance site at 39.1 AU. Crests of the waves are white; the greyscale is stretched to reveal the contrast. The surface density amplitude can be found from eqn (43). The first wavelength is 75 AU, in agreement with the $\mu_d/\mu_s = 1$ curve of figure 6, and decreases as $r^{-1/2}$. These waves are predicted to become non-linear at ~ 330 AU, which is near the edge of the plot.









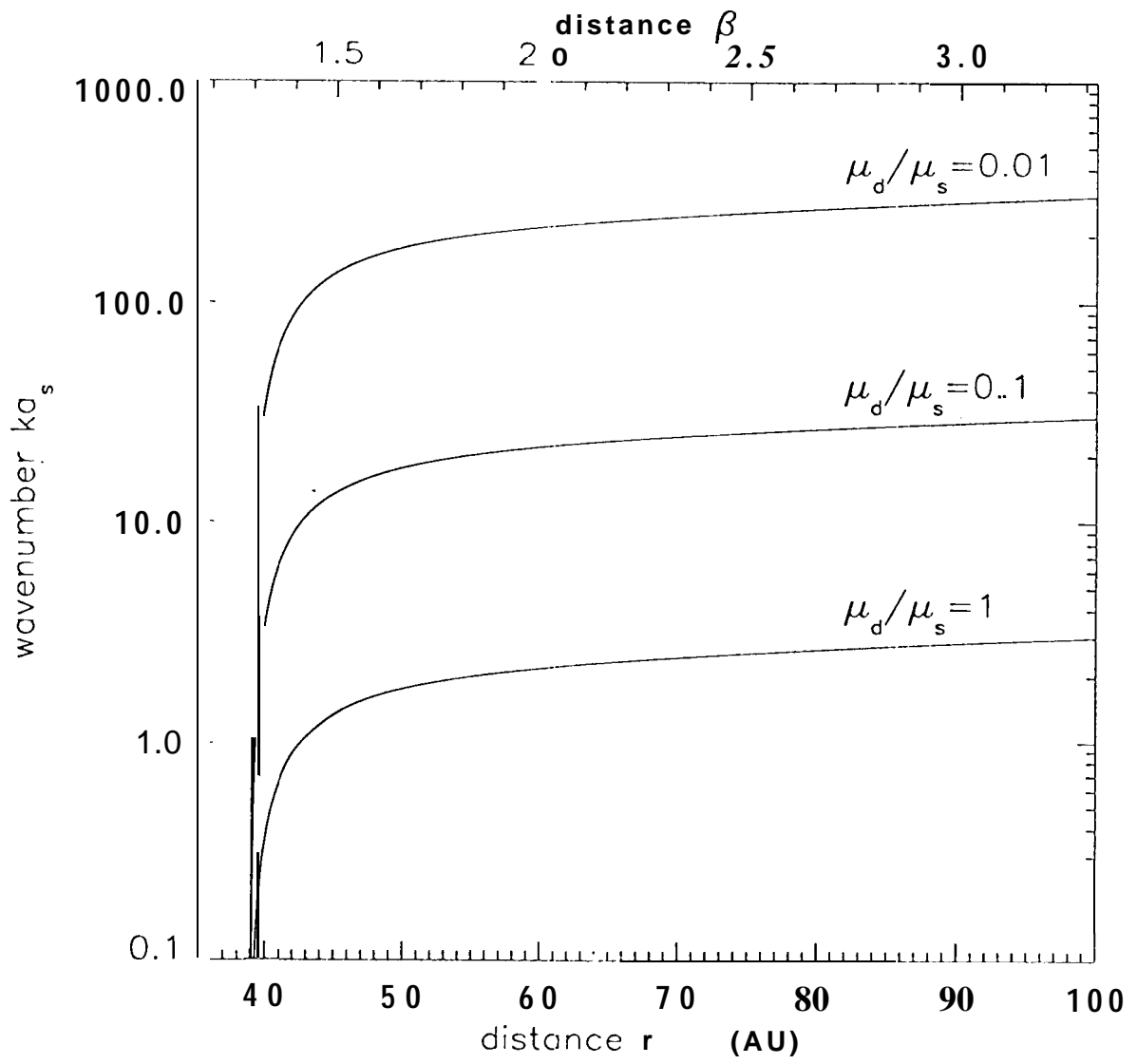


Fig 5

